

## Probing hadronic cosmic ray acceleration in infrared bright SNRs with Fermi-LAT

Pranjupriya Goswami,<sup>a,b,\*</sup> Enrique Mestre,<sup>c</sup> Iurii Sushch,<sup>a,d</sup> Emma de Oña Wilhelmi<sup>e</sup> and Robert Brose<sup>f</sup>

<sup>a</sup>Centre for Space Research, North-West University, Potchefstroom, 2520, South Africa

<sup>b</sup>Université Paris Cité, CNRS, Astroparticule et Cosmologie, F-75013 Paris, France

<sup>c</sup>Institute of Space Sciences (ICE/CSIC), Campus UAB, Carrer de Can Magrans s/n, 08193, Barcelona, Spain

<sup>d</sup>Astronomical Observatory of Ivan Franko National University of Lviv, Kyryla i Methodia 8, 79005 Lviv, Ukraine

<sup>e</sup>Deutsches Elektronen Synchrotron DESY, 15738 Zeuthen, Germany

<sup>f</sup>Dublin Institute for Advanced Studies, Astronomy & Astrophysics Section, 31 Fitzwilliam Place, D02 XF86 Dublin 2, Ireland

E-mail: [goswami@apc.in2p3.fr](mailto:goswami@apc.in2p3.fr), [iurii.sushch@nwu.ac.za](mailto:iurii.sushch@nwu.ac.za)

Recent Fermi-LAT observations have revealed the signature of proton acceleration and hadronic emission at GeV energies in various SNRs, possibly due to the interaction with molecular clouds (MCs) in their surroundings. The hadronic interaction is evidenced by a characteristic spectral feature known as the pion-decay bump at energies from hundreds of MeV to a few GeV. We conducted a detailed spectral study with Fermi-LAT of 9 infrared bright SNRs detected by SPITZER, in which, presumably, particle interaction with the high-density medium favourable for the hadronic emission of gamma-rays occurs. We explain the observed GeV emission in the context of the cosmic ray interaction with the ambient gas, probing the rapid decrease of the maximum energy accompanied by the particle escape, characteristic of old dynamical age, as well as the potential contribution of heavy nuclei, which are in abundance in the circumstellar medium that surrounds core-collapse SNRs. We also report on the potential detection of a few undetected sources in the Fermi-LAT Supernova remnant catalog.

38th International Cosmic Ray Conference (ICRC2023)  
26 July - 3 August, 2023  
Nagoya, Japan



\*Speaker

## 1. Introduction

Supernova remnants (SNRs) have long been recognized as the primary candidates for production of Galactic cosmic rays. Although the evidence of acceleration to PeV energies needed to explain the ‘knee’ feature in the cosmic-ray spectrum is elusive it is clear that particles can be accelerated to relativistic energies at SNR shocks through the diffusive shock acceleration. Accelerated protons and heavier nuclei subsequently interact with the surrounding matter, including dense molecular clouds (MCs), resulting in the generation of  $\pi^0$  mesons that subsequently decay into  $\gamma$ -rays. The spectral energy distribution (SED) of hadronic gamma-ray sources exhibits a distinctive pion-decay bump, characterized by a rising spectrum below 200 MeV followed by a hard component extending up to the maximum energy. This characteristic spectral feature directly indicates the signature of proton-proton interactions. This feature can be used to differentiate hadronic scenarios from leptonic mechanisms of gamma-ray emission production such as inverse Compton (IC) scattering and/or bremsstrahlung. Identification of hadronic accelerators among SNRs is important in the view of understanding the origins of cosmic rays that consist mainly of protons.

Recent observations by the Fermi Large Area Telescope (LAT) have revealed this characteristic hadronic spectrum for several supernova remnants, including IC 443, W44, W49B, W51C, and HB 21 [6, 8, 9] indicating their interaction with molecular clouds. In a comprehensive study of 4FGL catalog sources situated within  $5^\circ$  from the Galactic plane, the Fermi-LAT collaboration [6] confirmed 13 SNRs, such as G31.9+0.0, G43.3-0.2, G304.6+0.1, G054.4-0.3, G329.7+0.4, and Kes 79, exhibiting spectral breaks at low energies ranging between 100 MeV and 550 MeV. They interpreted this emission as arising from proton-proton interactions enhanced by the presence of dense target material. More recently, de Oña Wilhelmi et al. (2020) [10] reported gamma-ray studies of SNR G39.2-0.3 (a core-collapse Type IIL/b supernova), one of the brightest SNRs in infrared and gamma-rays, and an exemplary accelerator of GeV hadronic cosmic rays. The Fermi-LAT spectrum for this SNR is well described by a log-parabola function, exhibiting a significant spectral break at an energy of 2.3 GeV. The authors conducted a thorough spectral modeling, considering both hadronic- and leptonic-induced scenarios to reproduce the observed gamma-ray spectrum, favouring hadronic interactions as the origin of the GeV emission.

In this work, we utilize LAT (Pass 8) data spanning 14 years to conduct a (re-)analysis of 9 infrared bright supernova remnants, selected from the GLIMPSE Legacy science program on the Spitzer Space Telescope [2], as listed in Table 1. The gamma-ray spectra of these SNRs potentially exhibit pion-decay signatures, suggesting proton-proton interactions. Some of these SNRs are supposedly core-collapse Type-II/b SNe, which undergo a red supergiant (RSG) phase, creating a rich and highly inhomogeneous medium in which the remnant expands. Their association with molecular clouds implies a potential for luminous gamma-ray emission. Among the listed SNRs, G31.9+0.0, G43.3-0.2, G304.6+0.1, G332.4-0.4, and G054.4-0.3 show clear evidence of H<sub>2</sub> and CO emission lines and interact with dense molecular clouds. However, the interactions for SNRs G310.8-0.4 and G311.5-0.3 remain unknown. Our primary aim is to study the gamma-ray emission from these SNRs and understand the mechanisms responsible for their unique spectral features.

**Table 1:** Our sample of infrared bright SNRs.

SNR / counterpart	GLON/GLAT	Age	Detection	Interaction	4 FGL association
G31.9+00.0/3C391	31.860/ 0.018	7400 - 8400 yr	Fermi	CO, HI	J1849.4-0056
G41.1-00.3 / 3C397	41.110/ -0.310	~ 5000	Fermi (?), H.E.S.S. (?)	LB (CO, HCO+)	
G043.3-00.2 / W49B	43.251/ -0.176	2900 - 6000 yr	Fermi, H.E.S.S.	HI	J1911.0+0905
G304.6+00.1 / Kes 17	304.554/ 0.133	2000-64000 yr	Fermi	HII	J1305.5-6241
G332.4-00.4/ RCW 103	332.428/ -0.363	2000-4400 yr	Fermi	HII	–
G054.4-00.3 / HC40	54.470/ -0.290	61000 yr	Fermi	CO, HI	J1934.3+1859
G310.8-00.4 / Kes 20A	310.8/ -0.4	–	Non-detection	–	–
G311.5-00.3	311.5/ -0.3	–	Non-detection	–	–
G346.6-00.2	346.6/ -0.2	4200-16000	Non-detection	OH, HII	–

References: Column 1,2,3: [SNRcat](#); Column 4,6; 4FGL Catalog [4], Column 4,5: 1st Fermi-LAT SNR Catalog [3]

## 2. Observations and Data analysis

We selected Fermi-LAT events inside the  $15^\circ \times 15^\circ$  regions centered at the positions of the SNRs listed in Table 1 from the Fermi Pass 8 (P8R3) public database [1]. The LAT data we downloaded spans in time from 2008/09 to 2022/09. The publicly available software `FERMITOOLS` (version 2.0.8) and the `PYTHON` package `FERMIPY` (version v1.0.1) were used to analyze the data. We selected only `EVENT` class data (P8R3 `SOURCE`) and type 3 events (i.e., `FRONT+BACK` events) and applied standard data quality selection criteria (`DATA_QUAL > 0 && LAT_CONFIG == 1`) for analyzing the dataset. The zenith angle was restricted to a maximum of  $90^\circ$  to avoid contamination due to the Earth’s limb. We used the latest versions of the instrument response functions (IRFs, version `P8R3_SOURCE_V2`), the diffuse Galactic interstellar emission (`gll_iem_v07.fits`), and the isotropic emission (`iso_P8R3_SOURCE_V2_v1.txt`) models. In the background model, we included all sources listed in the recent fourth Fermi-LAT source catalog (data release 3, 4FGL-DR3) [5]. We rejected events below 100 MeV because of the relatively large uncertainties of the LAT instrument response functions in the low-energy range, limiting the analysis to energies from 0.1 to 300 GeV.

### 2.1 Source identification:

The sources G31.9+0.0, G43.3-0.2, and G304.6+0.1 are well detected by Fermi and included in the 4FGL catalog [4] as point-like sources. For modeling our regions of interest (ROIs), consisting of  $15^\circ$  radii centered at the positions of the SNRs, we included all sources located within the ROIs in the Fermi 4th source catalog (4FGL, [4]). The LAT sources’ positional information and spectral functional forms (*LogParabola*) were adopted as provided in the same catalog. To fit the ROI model to the data, we left free to vary the spectral parameters and normalization of all sources within  $5^\circ$  from the SNRs. We fixed the rest of the parameters of the ROI sources to their catalog values. The normalization and tilt of the Galactic diffuse emission and the normalization of the extragalactic diffuse emission models are also free parameters of the ROI models. To analyze the LAT data, we conducted standard binned likelihood analyses and extracted the Test Statistic (TS) maps of  $5^\circ \times 5^\circ$  regions centered at the positions of the SNRs. The source TS values are estimated as  $TS = 2 \log(\mathcal{L}_1/\mathcal{L}_0)$ , where  $\mathcal{L}_1$  and  $\mathcal{L}_0$  are the likelihoods obtained by fitting the model to the data if including a test source and without the source. TS maps around the sources of interest overlaid with the

available radio maps of the SNRs are shown in Figure 1. We report the sources' TS values at 1 GeV of energy in Table 2. It is noticeable from the TS maps that some of the SNRs are located in very complex regions. We used the `FERMIPY LOCALIZE` and `EXTENSION` methods to optimize the sources' positions and to probe for possible extended emissions from the sources. The `LOCALIZE` method optimizes the position of a source, scanning the likelihood surface around a putative location. The `EXTENSION` method employs a Gaussian spatial model to compare the extended and no-extended (point-source) hypotheses through the likelihood ratio test.

SNR G41.1-0.3 is not included in the 4FGL catalog, being the source located in a very complex region with the LAT sources 4FGL J1906.9+0712 and PSR J1906+0722 (4FGL J1906.4+07234) in very close proximity. We modeled G41.1-0.3 as a point-like source at the location of its radio position and assuming a *LogParabola*-type spectrum. We considered the LAT 4FGL nearby sources in the background model and fit the data assuming the spectral shapes listed in the 4FGL catalog, obtaining  $\sim 8\sigma$  at the source location. See a TS map of the source in Figure 1.

In the SNR G332.4-0.4 (RCW 103) case, we noted two nearby sources; PSR J1617-5055 and the H.E.S.S. source HESS J1616-508 (4FGL J1616.2-5054e). The H.E.S.S. source is an extended pulsar wind nebula (PWN) powered by PSR J1617-5055. We considered a point-like source at the location of its radio position with a *LogParabola*-type spectrum to account for RCW103 in the ROI. Including both PSR J1617-5055 and HESS J1616-508 in the background model, we obtained a  $\sim 27\sigma$  gamma-ray excess at the location of RCW 103.

SNR G054.4-0.3 is associated with the LAT source 4FGL J1934.3+1859. The radio counterpart has a shell-type morphology with a nearly circular shape and angular diameter of  $\sim 40$  arcmin. The young gamma-ray pulsar PSR J1932+1916 (4FGL J1932.3+1916) lies at the near edge of the remnant. We modeled 4FGL J1934.3+1859 as a point-like source with a log-parabola spectrum achieving  $14.5\sigma$  of detection significance. An exponential cutoff power-law model for the source's spectrum did not improve the likelihood of the ROI model. We also probed the extended source hypothesis, which resulted in moderate hints of extension with  $\sim 0.3^\circ$  for the 68% containment radius. 4FGL J1932.3+1916, detected at very large significance ( $\sim 56\sigma$ ), is best-fit to a point-like source with a sub-exponential cutoff power-law spectrum and  $0.83 \pm 0.15$  GeV of cutoff energy. Still, we observed faint (residual) LAT emission along the whole limb of the remnant's radio shell. We accounted for the same by fitting a (template) diffuse source (at  $\sim 5.7\sigma$ ) with a radial shell morphology of  $0.23^\circ/0.38^\circ$  of inner/outer radius centered at  $l = 54.5^\circ$  and  $b = -0.26^\circ$  and a power-law spectrum of  $1.9 \pm 0.2$  index.

The SNRs G310.8-0.4 (Kes 20A) and G311.5-0.3 are located in a very complex region, close to each other with an angular separation of  $0.6^\circ$  and in the vicinity of the SNR Kes 20B (4FGL J1358.2-6210) and the unidentified LAT source dubbed 4FGL J1404.4-6159. These SNRs have been reported as LAT undetected sources in the 1st Fermi-LAT SNR Catalog [3]. To analyze the LAT data towards the remnants, we included G310.8-0.4 and G311.5-0.3 in the ROI model, both as point-like sources at their radio locations and assuming *power-law* spectral models. We include all 4FGL catalog sources in the ROI to account for the background and left free to vary the spectral parameters of all sources within  $5^\circ$  from the nominal positions. After the ROI model fitting, we obtained only  $\sim 4.04\sigma$  at the location of Kes 20A and  $\sim 3.83\sigma$  for G311.5-0.3. However, the SNRs Kes 20A and 20B are located in very close proximity with an angular distance of  $\sim 0.3^\circ$ . Hence, a relation between Kes 20A and the LAT source 4FGL J1358.2-6210 can not be completely ruled

out. We also estimated the angular separation between the best-fit positions of G311.5-0.3 and 4FGL J1404.4-6159, which is only  $0.23^\circ$ . Therefore, it is possible that the SNR is associated with the LAT source 4FGL J1404.4-6159. We obtained a  $TS \sim 17.3\sigma$  for 4FGL J1404.4-6159 and a soft spectrum ( $\alpha=3.12$  at  $E_b=1.5$  GeV) following a *LogParabola* spectral shape, resembling the spectrum of SNRs of the type examined.

Finally, G346.6-0.2 is a shell-type Galactic SNR positioned in the vicinity of the extended SNR RX J1713.7-3946 (4FGL J1713.5-3945e), with the region being abundant in clouds. We modeled G346.6-0.2 as a point-like source in our analysis, employing both *PowerLaw* and *LogParabola* spectral models. However, we could not detect the source using any of these models, obtaining only an excess at less than  $3\sigma$  at the source's location.

### 3. Spectral results

For the 4FGL sources, we used the spectral model defined in the catalog[4], which is a *LogParabola* (LP). To fit the ROIs, we applied the above mentioned criteria, freeing the spectral parameters of all sources within a  $5^\circ$  radius around the sources of interest. The SEDs were then generated using the best-fit model parameters and the standard SED method in FERMIPY with three bins per energy decade. As for the manually added sources (not included in 4FGL), we performed iterative tests for each to assess the improvement of the log-normal representation compared to the *PowerLaw* (PL) form. A significant improvement (at least by  $3\sigma$ ) was observed by incorporating the LP model in place of PL, as determined by  $TS(LP) = 2 \log(\mathcal{L}(LP) - \mathcal{L}(PL))$ . The LP spectral parameters,  $\alpha$  (at  $E_b \sim 1$  GeV),  $\beta$ , and integrated flux in the entire energy range, are reported in Table 2. The spectral points are shown in Figure 2.

We next tested a smoothly broken PL (SBPL; *SmoothBrokenPowerLaw*) model, which added two additional degrees of freedom compared to the PL model (the break energy  $E_{br}$  and a second spectral index  $\Gamma_2$ ) [6]. In contrast to the LP model, we do not observe significant improvement in the likelihood value. Nevertheless, the SBPL model provides a quantitative idea of the spectral breaks, and all the sources show a significant energy break in their low-energy spectrum, as reported in Table 2. In addition, we tested a PL with an exponential cutoff (PLEC) model, which is included as *PLSuperExpCutoff* under *SpectrumType* in the 4FGL catalog [4], as some of the SNRs SEDs show significant curvature. This model can be useful to avoid having newly added sources overlap with pulsars. Even though the model doesn't provide a satisfactory fit to the data (no improvement in the TS compared to a *LogParabola*), it provides a rough estimate of the cutoff energies, as reported in Table 2.

### 4. Interpretation of $\gamma$ -ray spectrum and discussion

Given the presumed hadronic origin of the observed gamma-ray spectra, we employ a similar approach to that used in de Oña Wilhelmi et al. (2020) [10]. To calculate the gamma-ray spectrum due to pion decay, we use a module in the post-processing radiation routine of the RATPaC code (see [11–13] for details). The module uses pre-calculated inelastic cross-sections and differential production rates of secondary particles produced in nuclei collisions based on Monte Carlo event

**Table 2:** The best-fit parameters for the LP, SBPL, and PLEC models.

SNR	$\sqrt{TS}_{LP}$	$\alpha$	$\beta$	Flux (0.1-300 GeV) ( $10^{-8}$ ph cm $^{-2}$ s $^{-1}$ )	$E_{br,SBPL}$ (GeV)	$E_{cutoff,PLEC}$ (GeV)	Extension (deg)
G031.9+00.0	30.62	$2.24 \pm 0.07$	$0.17 \pm 0.006$	$4.35 \pm 0.017$	$2.3 \pm 0.08$	$14.09 \pm 0.75$	$0.13^{+0.019}_{-0.014}$
G041.1-00.3	8.12	$2.55 \pm 0.03$	$0.24 \pm 0.0020$	$5.53 \pm 0.08$	$1.71 \pm 0.02$	$6.84 \pm 0.71$	$0.12^{+0.014}_{-0.013}$
G043.3-00.2	82.23	$2.26 \pm 0.005$	$0.12 \pm 0.002$	$15.49 \pm 0.034$	$1.9 \pm 0.02$	$26.25 \pm 0.51$	$0.074^{+0.009}_{-0.005}$
G304.6+00.1	27.28	$2.32 \pm 0.03$	$0.0078 \pm 0.013$	$7.67 \pm 0.06$	$0.44 \pm 0.017$	$126.5 \pm 1.45$	$0.114 \pm 0.012$
G332.4-00.4	11.06	$1.92 \pm 0.01$	$0.097 \pm 0.005$	$4.66 \pm 0.013$	$2.3 \pm 0.59$	$26.29 \pm 0.14$	$0.25^{+0.028}_{-0.025}$
G054.4-00.3	14.5	$3.05 \pm 0.20$	$0.51 \pm 0.08$	$3.47 \pm 0.75$	$0.35 \pm 0.03$	$0.82 \pm 0.14$ GeV	$0.31^{+0.007}_{-0.008}$

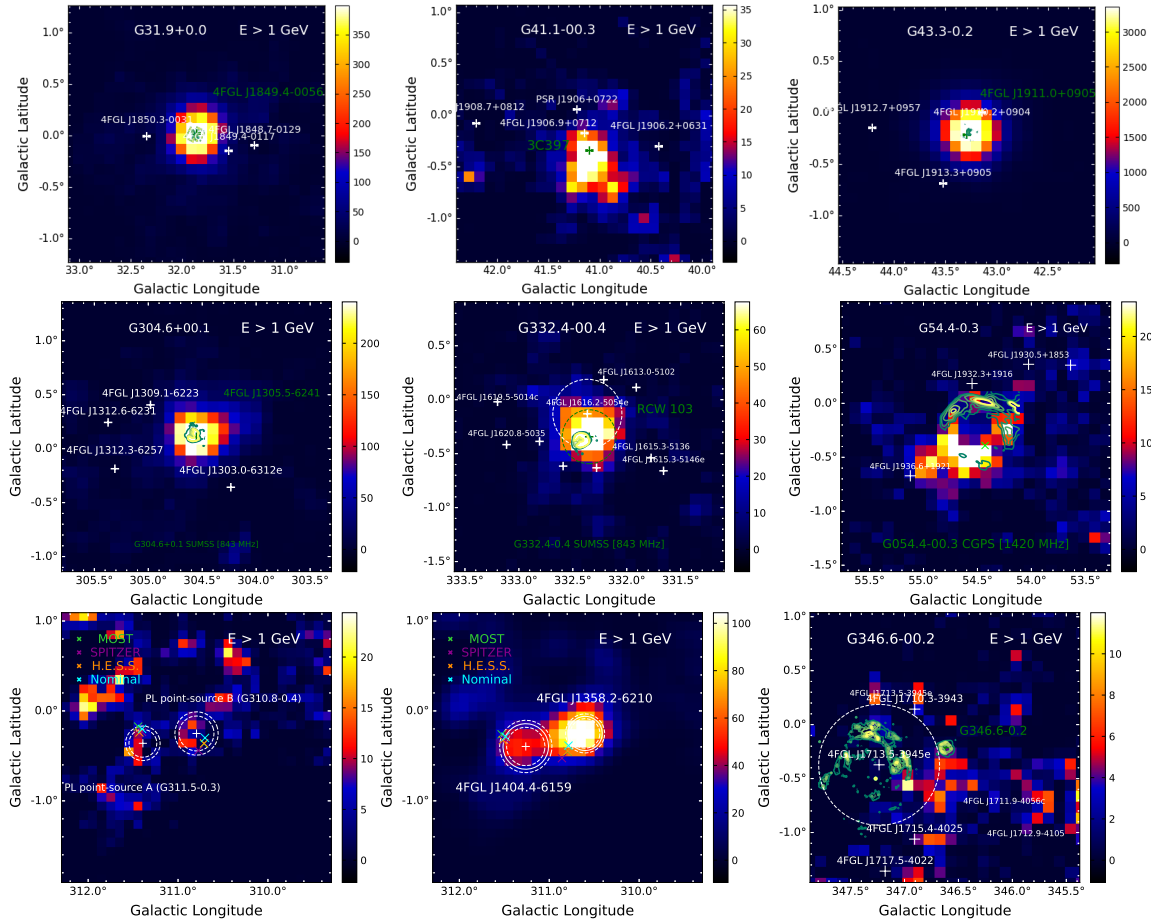


**Figure 1:** Source TS maps at energies above 1 GeV overlaid with radio contours. The TS maps of SNRs G310.8-0.4 and G311.5-0.3 are shown in the first two plots from the left in the bottom panel. The left plot corresponds to the residual map after fitting the 4FGL sources J1358.2-6210 and J1404.4-6159. The middle plot shows the source TS maps of the cited 4FGL sources in the vicinity of the SNRs location.

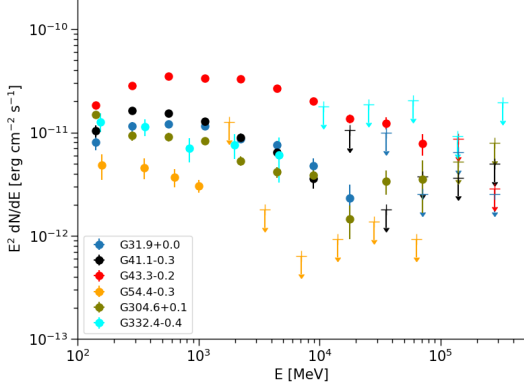


**Figure 2:** Spectral energy distributions of the SNRs G31.9+0.0, G41.1-0.3, G43.3-0.2, G304.6+0.1, G332.4-0.4, and G054.4-0.3 fitted with a *LogParabola* model. The best-fit parameters are listed in Table 2.

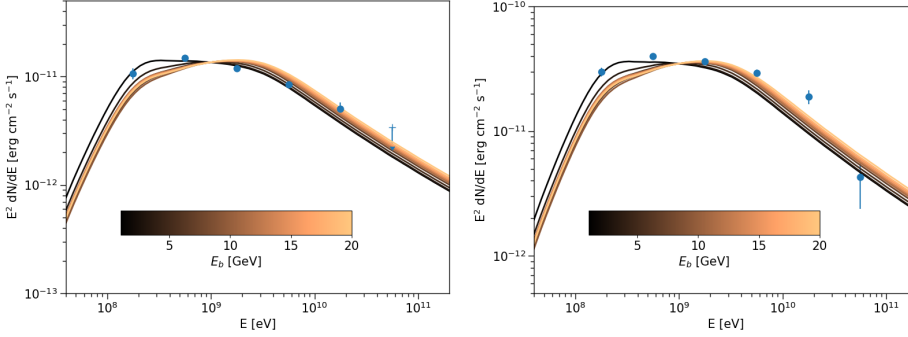


**Figure 3:** Spectral energy distributions and modeled hadronic gamma-ray emission from the SNRs with a broken power-law distribution of protons.  $s_1=2.0$ ,  $s_2=2.6$  (fixed) and  $E_b$  varying between 1 and 20 GeV. Left: **G031.9+00.0**: used params:  $R=7\text{pc}$ ,  $d=7.2\text{kpc}$ , density= $387\text{ cm}^{-3}$  and normalization  $1.3\text{e-}11$  Right: **G043.3-00.2**: used params:  $R=6.4\text{pc}$ ,  $d=10\text{kpc}$ , density $\sim 500\text{ cm}^{-3}$  and normalization  $3.5\text{e-}11$

generators, DPMJETIII and UrQMD [14]. We calculate the expected gamma-ray emission from a toy proton spectrum in a broken power-law form in momentum, given as,

$$\frac{dN}{dp} = \begin{cases} N_0 p^{-s_1}, & \text{if } p \leq p_b \\ N_0 p_b^{-s_1+s_2} p^{-s_2}, & \text{otherwise} \end{cases}$$

Here  $p_b$  is the break momentum associated with energy  $E_b$ .

We initially applied this code to the gamma-ray spectrum of two SNRs; G31.9+0.0 and G43.3-0.2, for which the gamma-ray emission is well described by hadronic interactions and vary the fitting parameters as in de Oña Wilhelmi et al. (2020) [10]. To see how the spectral shape changes with the break energy  $E_b$ , we fix spectral indices to  $s_1 = 2.0$  (motivated by diffusive shock acceleration, DSA) and  $s_2 = 2.6$ . and vary  $E_b$  from 1-20 GeV. The SED models are shown in Fig. 3.

The shape of the observed gamma-ray spectrum is characteristic for the hadronic origin of the gamma-ray emission for dynamically old SNRs. The soft spectrum at higher energies could be attributed to the decrease of the maximum achievable energy in the particle acceleration process with time, while the break in the spectrum reflects the maximum achievable particle energy at the

current stage of evolution as described in [15]. The models presented in Fig. 3 prefer rather low break energies of  $\sim 1$  GeV, implying a quite old dynamical age of remnants.

To summarize, this contribution presents preliminary results from the Fermi-LAT analysis of 9 infrared bright SNRs. Among them, five SNRs (G31.9+0.0, G41.1-0.3, G43.3-0.2, G304.6+0.1, G332.4-0.4, and G054.4-0.3) are well-detected by Fermi-LAT, and their gamma-ray spectra exhibit significant breaks at low energies ranging from 0.4 to 2.3 GeV. Further, we observe a likely association of these SNRs with 4FGL sources in our analysis, as discussed in section 2.1. For the bright gamma-ray SNRs, we employed various spectral models, however, all the spectra appeared to resemble a curved LogParabola spectrum, providing significantly improved test statistics over other spectral models. Nonetheless, our work is ongoing to confirm the detections of the faint SNRs (G310.8-0.4 and G311.5-0.3). Additionally, we attempted to explain the gamma-ray emissions using the pion decay module available in the RATPaC code (ref. to the discussion in section 3), which allows us to derive the gamma-ray emission produced by proton-proton interactions. The model successfully reproduced the SEDs of two SNRs, G31.9+0.0 and G43.3-0.2. In future work, we plan to apply this model to all SNRs and provide a detailed interpretation of the origin of  $\gamma$ -rays in terms of hadronic interactions.

#### Acknowledgement:

I. Sushch acknowledges support by the National Research Foundation of South Africa (Grant Number 132276). Authors thank the Fermi Science Support Center (FSSC) team for providing the data and analysis tools.

#### References

- [1] Atwood, W., Albert, A., Baldini, L., et al. 2013; [arXiv:1303.3514](#)
- [2] Reach et al. 2006, [ApJ](#), 131, 3
- [3] Acero, F., Ackermann, M., Ajello, M., et al. 2016, [ApJS](#), 224, 8
- [4] Abdollahi, S. et al. for the Fermi-LAT collaboration, [ApJS](#) 247, 33, 2020
- [5] Abdollahi, S. et al. 2022, [ApJS](#), 260, 53
- [6] Abdollahi, S. et al., 2022, [ApJ](#), 933, 204
- [7] Jared Siegel et al 2020, [ApJ](#), 904, 175
- [8] H. E. S. S. Collaboration, Abdalla, H., Abramowski, A., et al. 2018a, [A&A](#), 612, A5
- [9] Ackermann, M., Ajello, M., Allafort, A., et al. 2013, [Science](#), 339, 807
- [10] de Oña Wilhelmi E., Sushch I., Brose R., et al., 2020, [MNRAS](#), 497, 3581
- [11] Telezhinsky I., Dwarkadas V. V., Pohl M., 2012, [Astroparticle Physics](#), 35, 300
- [12] Brose R., Telezhinsky I., Pohl M., 2016, [A&A](#), 593, A20
- [13] Sushch I., Brose R., Pohl M., 2018, [A&A](#), 618, A155
- [14] Bhatt M., Sushch I., Pohl M., et al., 2020, [Astroparticle Physics](#), 123, article id. 102490
- [15] Brose R., Pohl M., Sushch I., et al., 2020, [A&A](#), 634, A59